ADVANCED FUNCTIONAL MATERIALS
www.afm-journal.de

Protein Adsorption Modes Determine Reversible Cell Attachment on Poly(*N*-isopropyl acrylamide) Brushes

*Changying Xue, Byun-Chan Choi, Sangwook Choi, Paul V. Braun, and Deborah E. Leckband**

Protein adsorption and reversible cell attachment are investigated as a function of the grafting density of poly(*N*-isopropyl acrylamide) (PNIPAM) brushes. Prior studies demonstrated that the thermally driven collapse of grafted PNIPAM above the lower critical solution temperature of 32 °C is not required for protein adsorption. Here, the dependence of reversible, protein-mediated cell adhesion on the polymer chain density, above and below the lower critical solution temperature, is reported. Above 32 °C, protein adsorption on PNIPAM brushes grafted from a non-adsorbing, oligo(ethylene oxide)-coated surface exhibits a maximum with respect to the grafting density. Few cells attach to either dilute or densely grafted PNIPAM chains, independent of whether the polymer brush collapses above 32 °C. However, both cells and proteins adsorb reversibly at intermediate chain densities. This supports a model in which the proteins, which support reversible cell attachment, adsorb by penetrating the brushes at intermediate grafting densities, under poor solvent conditions. In this scenario, reversible protein adsorption to PNIPAM brushes is determined by the thermal modulation of relative protein-segment attraction and osmotic repulsion.

1. Introduction

The temperature-dependent solubility of poly(*N*-isopropyl acrylamide) (PNIPAM) is broadly exploited in a variety of applications including viscosity modification, sensing,[1–3] drug targeting,[4,5] chromatography,[6–9] and cell sheet engineering for tissue regeneration.[10–18] PNIPAM undergoes a solubility transition at the lower critical solution temperature (LCST) of 32 °C. Relatively dense PNIPAM brushes are water swollen below the LCST, but collapse above the LCST. Although this is the generally accepted model of PNIPAM behavior, other studies show that more dilute and/or low molecular weight, end-grafted PNIPAM brushes do not collapse above 32 °C.[19–21] Instead, the chains appear to remain extended at higher temperatures. To assess the importance of chain collapse, protein adsorption on brushes that collapse above the LCST was compared with those that do not. Those comparisons demonstrated that reversible protein adsorption above the LCST does not require polymer collapse, but is instead driven primarily by the temperature-dependent change in solvent quality and consequent changes in protein-segment interactions.[22]

Applications that exploit the LCST, in order to reversibly capture proteins or cells are founded on temperature-dependent interactions between proteins and PNIPAM-coated surfaces. However, the polymer properties and mechanisms governing reversible protein and cell adsorption have not been defined. Prior studies focused on polymer wettability,[23–26] polymer collapse behavior,[20,27,28] coating thickness,[24,26,29,30] polymerization method,[31,32] and the molecular weight and density of end-grafted PNIPAM.[19,22,33,34] The current lack of consensus on PNIPAM coating properties that insure optimum performance stems in part from the lack of understanding of mechanism(s) of protein adsorption, under both good and poor solvent conditions.

Theoretical studies analyzed different modes of protein and colloid adsorption to end-grafted polymers under both good and poor solvent conditions, as a function of molecular weight and grafting density.[35–39] Proteins can adsorb to brushes by three modes, depending on the protein dimensions, the protein–surface attraction, the polymer molecular weight (MW) and the grafting density Γ (chains per area) (**Figure 1**).[36,40] The grafting density is related to the distance between grafting sites σ, by $\Gamma = 1/\sigma^2$. When $2R << \sigma$, primary adsorption occurs when proteins can diffuse through the brush to adsorb to the grafting substrate, and the adsorbed amount will depend on the brush properties and magnitude of the protein–surface attraction (Figure 1a). At densities where $2R >> \sigma$, proteins may adsorb at the outer edge of the brush (Figure 1c; secondary adsorption), via attractive interactions with the polymer or long-range attraction to the grafting surface. At intermediate densities, the protein can penetrate the brush, but not to the grafting surface (Figure 1b; ternary adsorption).[35,36] Ternary adsorption is generally opposed by the osmotic penalty for protein insertion

C. Xue, B.-C. Choi, S. Choi, Prof. D. E. Leckband
Department of Chemical and Biomolecular Engineering
University of Illinois
600 South Mathews Laboratory
Urbana, IL 61801, USA
E-mail: leckband@illinois.edu
Prof. P. V. Braun
Department of Material Science and Engineering
University of Illinois
Green Street, Urbana, IL 61801, USA

DOI: 10.1002/adfm.201103056

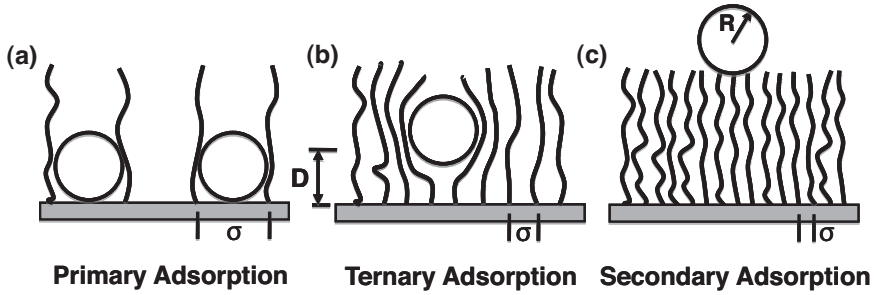

Figure 1. Protein adsorption modes on polymer brushes.

into the brush, but under poor solvent conditions, attractive segment–particle interactions may overcome the osmotic repulsion, to enable protein penetration.[35] So far, the mechanism(s) underlying reversible protein adsorption to PNIPAM coatings has not been determined.

These investigations compared protein and cell adhesion on end-grafted PNIPAM brushes with similar molecular weights but different chain grafting densities. Our previous study showed that the grafting density, rather than the molecular weight, has the greatest effect on protein adsorption at low molecular weight.[22] There are two important features of the brushes used in this study. First, we co-grafted PNIPAM with oligo(ethylene oxide)-silane (OEG), which suppresses primary protein adsorption (see Figure 1a), but still allows for secondary and ternary adsorption. This differs from several prior studies that used protein-adsorptive grafting substrates, and thereby enabled us to eliminate primary adsorption and explicitly test whether proteins and adhering cells interact directly and reversibly with the polymer chains via either secondary or ternary adsorption. The PNIPAM grafting density Γ was then varied over an order of magnitude, while keeping the MW similar at ≈40 kDa.

The second feature of these brushes is that some of the brushes synthesized do not collapse above the LCST. Several prior studies by us and by others demonstrated that dilute or low molecular weight chains remain extended in water above 32 °C, in contrast to the widely held view that PNIPAM always collapses.[19,20,22,27,28,34] This behavior also enabled us to test whether chain collapse above the LCST and re-swelling below the LCST are required for reversible protein and cell adsorption.

Here we show that, below the LCST, protein adsorption and cell attachment are negligible and independent of Γ. However, under poor solvent conditions (temperature $T >$ LCST), the dependence of protein adsorption on grafting density indicates that proteins attach to the brushes through ternary adsorption (see Figure 1). There is no evidence for secondary adsorption at high grafting densities, regardless of whether the brushes collapse. Comparisons of protein adsorption with reversible cell adhesion further indicate that this ternary protein adsorption facilitates the thermally reversible attachment of cells and extracellular matrix proteins to the PNIPAM polymer. These results suggest the protein adsorption mechanism and corresponding PNIPAM grafting conditions that are most conducive to the efficient, thermally reversible capture of proteins and cells.

2. Results and Discussion

2.1. Grafted PNIPAM Films

The molecular weight and grafting density of PNIPAM brushes were estimated from the initiator density and dry brush thickness. X-ray photoelectron spectroscopy (XPS) measurements quantified the initiator densities prior to polymerization for all but the lowest initiator concentrations. At $\Gamma <$ ≈0.04 nm^{-2}, the Br peak was below the detection limit, so that the grafting density was estimated from the initiator:OEG ratio.[22] Comparisons of XPS spectra before and after polymerization (**Figure 2**) confirmed the appearance of the nitrogen peak, indicative of PNIPAM on the surface. The PNIPAM grafting densities were then assumed to be 10% that of the initiator density, based on the results from polystyrene syntheses.[41,42] The dry polymer thicknesses were determined by ellipsometry (**Table 1**). Polymers grafted from the most dilute initiator monolayers were thin, and difficult to quantify reliably.

Table 1 summarizes the estimated grafting conditions and molecular weights of the thus prepared PNIPAM coatings. The

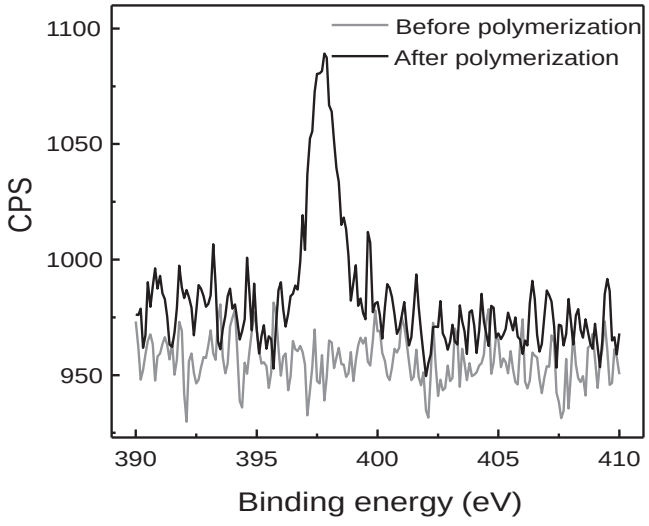

Figure 2. Nitrogen XPS spectrum of the initiator monolayer assembled from an initiator:OEG mixture at a 1:100 ratio before (light gray line) and after (black line) polymerization.

Table 1. Summary of Poly(*N*-isopropylacrylamide) Brush Parameters.

Estimated Grafting Density, Γ [chains nm^{-2}]	Dry Thickness [Å]	Estimated Molecular Weight [g mol^{-1}]	Degree of Polymerization	R_F [Å]	σ [Å]	$\sigma/(2R_F)$	Configuration
0.21[a)]	141 ± 5	38 500	341	99	22	0.11	brush
0.11[a)]	85 ± 8	44 000	389	107	30	0.14	brush
0.09	75 ± 7	48 000	425	113	33	0.15	brush
0.04	31 ± 5	44 000	392	108	50	0.23	brush
0.0105	5 ± 3	27 000	239	80	98	0.61	weak overlap
0.0021	1 ± 3	27 000	239	80	218	1.36	mushroom

[a)]Brushes are collapsed above 32 °C

For comparison, BSA dimensions: approximated as an equilateral triangular with 80 Å edges and 30 Å thickness.[45]

chain density in each case was estimated from the XPS data, the maximum packing density of 2.1 bromine initiator nm^{-2}, and a chain initiation efficiency of ≈10%, reported for polystyrene.[41,42] The molecular weight of the grafted PNIPAM was estimated from

$$M_n = \frac{h\rho N_A}{\sigma} \quad (1)$$

Here, h is the dry brush thickness (cm), ρ is the density of dry NIPAM (0.95 g cm^{-3}),[43] N_A is Avogadro's number, and Γ is the chain density (# cm^{-2}), which was estimated from the Br coverage and assumed initiator conversion efficiency. Based on these calculations, the estimated molecular weights of the majority of grafted PNIPAM in this study were similar at ≈40 kDa. The apparent, low molecular weight of 27 kDa on surfaces at grafting densities $\Gamma \approx 1.1 \times 10^{-2}$ and ≈2.1×10^{-3} chain nm^{-2} are due to the low initiator coverage or, more likely, to the large relative error in the film thickness determinations and unknown absolute value of the initiator density. Nevertheless, the use of the dilute initiator solutions i) reduced the chain density and hence the osmotic penalty for protein penetration of the grafted PNIPAM and ii) created conditions that enable primary adsorption to the OEG-coated grafting surface.

The configurations of the grafted polymers in good solvent were estimated from the calculated distance between grafting sites σ relative to the Flory radius $R_F = aN^{3/5}$,[44] assuming that water is a good solvent for PNIPAM at 23 °C. Here, a is the monomer length (≈3 Å)[19] and N is the polymerization degree. PNIPAM does not adsorb to hydrophilic, –OH terminated monolayers at $T > 32$ °C,[19] so it is reasonable to assume that PNIPAM does not adsorb to OEG monolayers. Based on the grafting densities and estimated MWs, the configurations at 23 °C include mushrooms, weakly overlapping chains, and stretched brushes (Table 1).

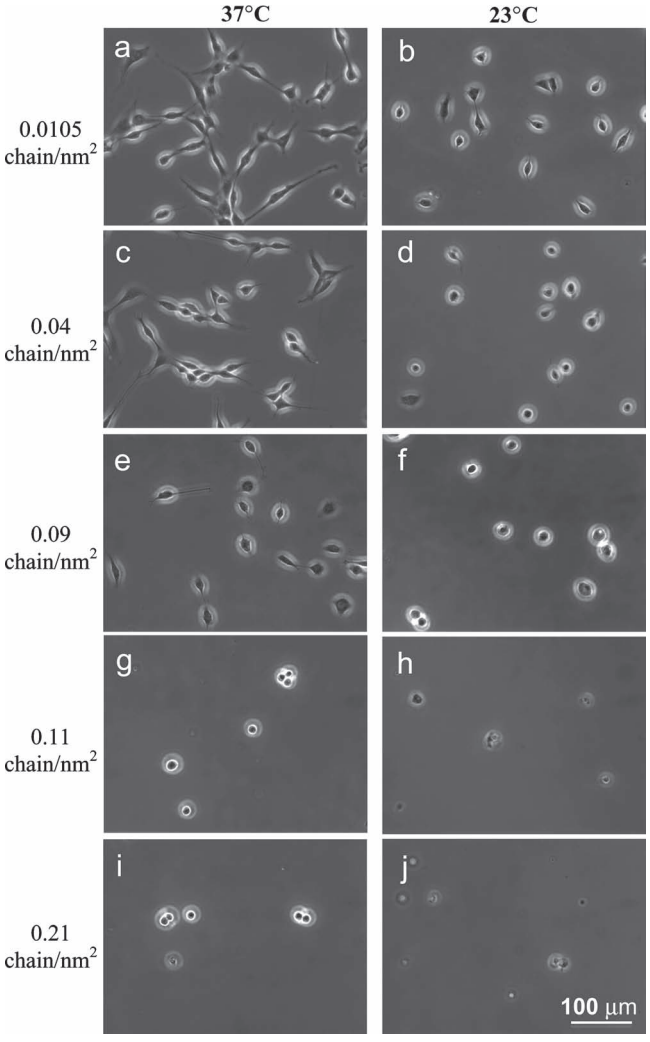

Figure 3. 3T3 fibroblast attachment at 37 °C on different PNIPAM brushes with similar molecular weight polymers. PNIPAM brushes were prepared on initiator monolayers with estimated grafting densities of a) 0.0105 chain nm^{-2}, c) 0.04 chain nm^{-2}, e) 0.09 chain nm^{-2}, g) 0.11 chain nm^{-2}, and i) 0.21 chain nm^{-2}. After 1 day in culture, the medium was replaced with room temperature L-15 medium, and cells were observed after 30 min at 23 °C on different PNIPAM brushes with grafting densities of b) 0.0105 chain nm^{-2}, d) 0.04 chain nm^{-2}, f) 0.09 chain nm^{-2}, h) 0.11 chain nm^{-2}, and j) 0.21 chain nm^{-2}.

2.2. Cell Attachment/Detachment on Thin PNIPAM Coatings

In order to assess the thermal reversibility of cell adhesion on the different polymer coatings, we observed 3T3 fibroblast attachment above and below the LCST. **Figure 3** shows the phase contrast images of cells cultured on five, different PNIPAM coatings, after 24 h in culture at 37 °C and then after

Table 2. Characterization of cells attached to PNIPAM coatings at 23 °C and 37 °C.

Γ [# nm^{-2}]	MW [kDa]	Cells per Area [# μm^{-2}]		Area per Cell [μm^2]		Circularity	
		37 °C	23 °C	37 °C	23 °C	37 °C	23 °C
0	na	29 ± 8	20 ± 4	418 ± 94	332 ± 51	0.59 ± 0.17	0.64 ± 0.16
0.0105	≈27	78 ± 7	45 ± 5	1162 ± 350	551 ± 163	0.35 ± 0.14	0.6 ± 0.18
0.04	44	66 ± 12	35 ± 4	762 ± 177	396 ± 123	0.37 ± 0.13	0.85 ± 0.12
0.09	48	37 ± 9	24 ± 5	590 ± 170	234 ± 59	0.46 ± 0.12	0.91 ± 0.03
0.11[a)]	44	15 ± 3	14 ± 4	254 ± 72	226 ± 52	0.93 ± 0.03	0.93 ± 0.03
0.21[a)]	38.5	16 ± 3	13 ± 3	249 ± 72	229 ± 56	0.93 ± 0.03	0.93 ± 003

[a)]Brushes are collapsed above 32 °C.

30 min at room temperature. At 37 °C, the cells attached and spread well on PNIPAM at the lower grafting densities. At the higher densities of ≈0.11 and ≈0.21 chain nm^{-2}, fewer cells attached and the remaining cells were more rounded, based on visual inspection and on calculated circularity (**Table 2**). Many of the cells on dense brushes formed intercellular aggregates, indicative of weak interactions with the substrate. At the intermediate grafting density of 0.09 chain nm^{-2}, the cell density was higher, but the spread areas were low and the circularity was high. Further decreasing Γ to 0.04 chain nm^{-2} and 1.05 × 10^{-2} chain nm^{-2} resulted in increased densities of attached, well-spread cells with correspondingly lower circularity.

These observations were quantified in terms of attached cell densities, spreading areas, and the cell circularity, as a function of film properties and temperature (Table 2). **Figure 4**a,b shows that both the density of attached cells and the spreading areas decreased with increasing PNIPAM grafting density, even though the denser brushes collapse above the LCST (Table 1). This agrees with a similar study of PNIPAM brushes,[33] and our results agree qualitatively with reports that cells attach to thin PNIPAM brushes, but not to thick films,[24,26,29,30,32,33] although direct comparisons between other coating methods and end-grafted PNIPAM are not always possible.

After replacing the warm medium (37 °C) with room temperature L-15 medium (23 °C), the cells were initially observed for 30 min. Control measurements showed that the change of medium and temperature does not affect fibroblasts on tissue culture plastic (Figure S.1, Supporting Information). The phase images in Figure 3b,d,f,h, and j show that the cell density on all of the PNIPAM coatings decreased, and the average cell circularity increased, indicative of cell detachment. This was especially apparent with PNIPAM brushes at Γ = 0.04 and 0.09 chain nm^{-2}. At Γ ≈ 0.0105 chain nm^{-2}, most of the cells rounded and started to float off the substrate within 30 min, and the circularity of the few remaining cells was high. A comparison of the quantified cell parameters at 37 °C with those after 30 min at ≈20 °C (Table 2; Figure 4), shows that, in all cases, lowering the temperature reduced cell–substrate adhesion. However, the efficacy of cell detachment within the first 30 min depended on the grafting parameters, such that cells detached more slowly from brushes that also adsorbed more protein.

Studies of cell detachment over longer observation times revealed that, despite differences in the percentage of cells that detached after 30 min, within ≈3 h, all cells on PNIPAM eventually rounded completely and detached at the lower temperature (Figure S.2, Supporting Information). Thus, apparent differences in the efficiency of cell release from the substrates used in this study are attributed to differences in protein and cell desorption kinetics, which depend on the polymer grafting density.

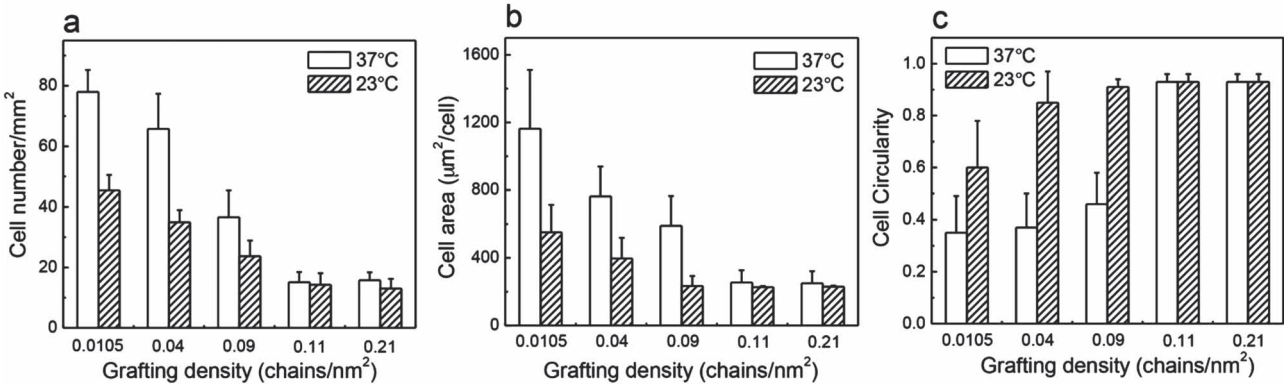

Figure 4. Characteristics of fibroblasts on different PNIPAM brushes at 37 °C and room temperature: a) number of cells per area, b) cell spreading area, and c) cell circularity.

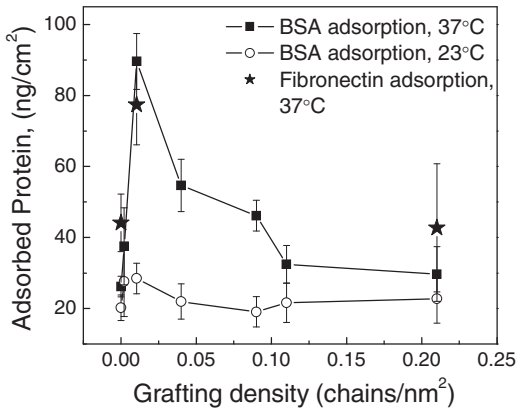

Figure 5. ^{125}[I]-labeled protein adsorption on PNIPAM brushes at 23 °C and at 37 °C. The polymer was grafted from initiator monolayers to produce brushes at the indicated grafting densities but with similar molecular weights of ≈40 kDa. Squares indicate ^{125}[I]-BSA adsorption at 37 °C. Circles show ^{125}[I]-BSA adsorption at 23 °C. The stars indicate ^{125}[I]-Fibronectin adsorption at 37 °C. The solid lines are to guide the eye.

2.3. Protein Adsorption Versus Grafting Density Γ

Figure 1 indicates the different protein adsorption modes, and their qualitative dependence on the PNIPAM grafting density Γ. The measured dependence of protein adsorption on Γ should therefore provide insights into the dominant mechanism(s) governing matrix protein adsorption, and hence cell adhesion, on PNIPAM brushes. To test this, we quantified ^{125}[I]-bovine serum albumin (BSA) adsorption as a function of Γ, at 37 °C and at 23 °C. In **Figure 5**, the BSA adsorption profile exhibits a maximum at $\Gamma \approx 0.0105$ chain nm^{-2}. Increasing or decreasing the PNIPAM density, relative to ≈0.0105 chain nm^{-2}, correspondingly reduced the adsorbed protein amount. By contrast, in good solvent at 23 °C, BSA adsorption was low on all PNIPAM brushes, and independent of Γ.

Because BSA may not represent the adsorption of extracellular matrix proteins, which support cell adhesion, we also quantified the adsorption of ^{125}[I]-fibronectin. The absolute adsorbed amount is slightly higher than BSA, but the fibronectin adsorption profile is qualitatively similar to BSA (Figure 5).

The maximum in protein adsorption versus the PNIPAM grafting density, in poor solvent, is strong evidence of ternary adsorption. Given the BSA dimensions (approximated as an equilateral triangular with 80 Å edges and 30 Å thickness)[45] relative to the estimated distance between PNIPAM chains, theory predicts that ternary BSA adsorption is feasible under these experimental conditions.[35–40,46] At the lowest chain densities where $2R < \sigma$ in good solvent, the OEG background prevents primary adsorption at both 25 °C and 37 °C, and the adsorbed amount is similar to that on OEG surfaces. There is also no secondary adsorption at the highest chain densities. The BSA adsorption at 37 °C and at intermediate grafting densities thus indicates protein-segment attraction and protein penetration of the brush, i.e., ternary adsorption.

It is important to note that the serum used in cell culture contains a wide range of proteins, which differ from BSA in size and physical properties, and may exhibit some differences in the adsorption behavior. However, the correlation between protein adsorption and cell adhesion measured in 10 v/v% serum (see below) suggests that any deviations are not large.

Osmotic repulsion generally opposes protein penetration of brushes (23 °C), but in poor solvent, increased segment-protein attraction may be sufficient to overcome the repulsion and enable protein insertion (Figure 1b).[37] Consistent with this view, at $T >$ LCST, protein adsorption increases with decreasing grafting density, which is the expected trend for ternary adsorption.[37] With PNIPAM brushes that adsorb protein but do not collapse above the LCST,[19,21,22,34,47,48] we attribute the reversible adsorption/release to the temperature-modulated balance between these attractive and repulsive terms. These results thus support a model in which proteins (and attached cells) reversibly adsorb to PNIPAM coatings that allow protein penetration into a brush-like outer layer.

2.4. Protein Adsorption Correlates with Cell Adhesion on PNIPAM Brushes

To test whether there is a causal relationship between the protein adsorption modes and cell adhesion, we compared BSA and fibronectin adsorption with cell attachment at both 37 °C and 23 °C. **Figure 6** shows that reversible cell attachment follows the same qualitative dependence on Γ and temperature as the single-component protein solutions. Namely, at 37 °C, cell attachment and spreading also exhibit a maximum, with few cells attaching to the most dilute or to the denser PNIPAM

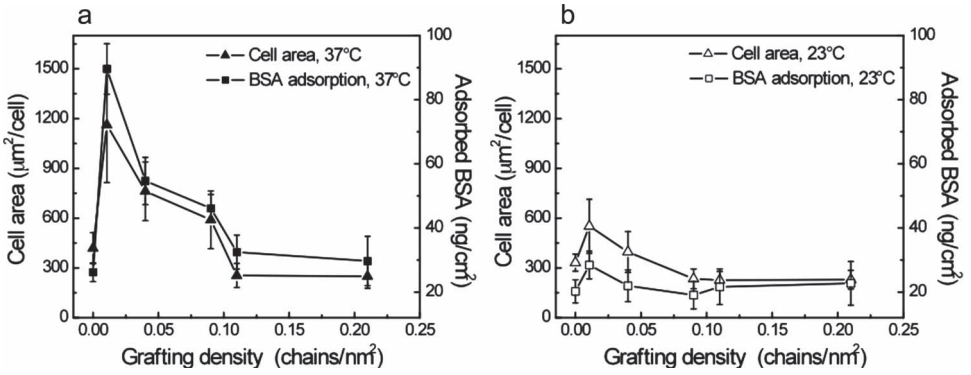

Figure 6. Comparison of fibroblast attachment (cell area, μm^2; triangles) and protein adsorption (ng cm^{-2}, squares) on PNIPAM brushes as a function of the grafting density at a) 37 °C and b) 23 °C.

chains. This confirms that BSA (and fibronectin) adsorption reports the physical chemical changes in protein interactions with the brushes that similarly govern extracellular matrix protein adsorption and cell adhesion. This correlation confirms that the protein adsorption mode is an important factor underlying reversible cell attachment.

2.5. Relationship to Prior Studies

Here, we used PNIPAM grafted from non-adsorbing surfaces using ATRP. However, PNIPAM coatings have also been prepared by other methods including plasma[25,49] and electron-beam polymerization.[24,26,32,50] In the case of electron-beam polymerization, cell adhesion depends on the film thickness, with fewer cells adhering to thick, cross-linked gels, and higher numbers adhering to thinner gels.[26] Plasma-polymerized films exhibit thermally reversible cell attachment, and it has generally been assumed, based on images of dry films, that their wet surfaces are smooth and comprise densely cross-linked chains.[25] However, there is currently little information about the architecture of the surfaces of wet, plasma-polymerized PNIPAM coatings. In another study, cells did not attach to thick, cross-linked polyacrylamide gels. The proposed explanation was that the gel proximal to the substrate is more hyodrophobic, but the outer region is more hydrated and protein resistant.[26] That explanation contrasts with our findings that more protein adsorbs to the more dilute PNIPAM brushes, which contain a greater volume fraction of water than dense chains.[21]

The present results instead provide compelling evidence that proteins undergo ternary adsorption on PNIPAM brushes at intermediate grafting densities. The OEG-coated substrates suppress primary adsorption, and there is no secondary adsorption on dense brushes, even though they collapse at $T >$ LCST (Figure 5; Table 1).[26,51] Our grafting substrates differ from other charged and nonpolar substrates that allow primary adsorption, so it may not be possible to generalize the adsorption profiles to all PNIPAM coatings. Ternary adsorption is still expected, but grafting substrates that allow primary adsorption would generate differences. PNIPAM adsorption to grafting substrates would also alter the chain configurations or even block primary adsorption, by competing with proteins for surface binding sites. Both would complicate determining the principal mechanisms governing protein adsorption. Our intentional use of a non-adsorbing, grafting substrate was, therefore, essential for identifying mechanisms of protein interactions with the PNIPAM. Such results provide a basis for both interpreting adsorption data and rationally designing coatings. These findings show that, above the LCST, proteins preferentially adsorb to relatively dilute PNIPAM chains that allow extensive, weak protein-segment interactions, rather than to dense, collapsed chains. We postulate that such polymer architecture is more conducive to thermally reversible cell attachment.

3. Conclusions

This study identified PNIPAM grafting conditions that support efficient, thermally reversible cell attachment to end-grafted PNIPAM brushes. Cell adhesion correlates directly with the dependence of protein adsorption on the chain density and exhibits a maximum at intermediate grafting densities, which is a key signature of ternary protein adsorption.[35] Below 32 °C, PNIPAM brushes are water-swollen and as protein- and cell-repellant as oligo(ethylene oxide) coatings. In poor solvent ($T >$ LCST), protein adsorption is negligible at high grafting densities, but exhibits a maximum at intermediate values. Furthermore, the protein and cell adsorption to brushes that do not collapse above the LCST indicates that neither brush collapse nor re-swelling is essential for reversible cell adhesion. Instead, polymer architectures that enable thermally modulated protein penetration of brush-like outer chains appear to exhibit the optimum properties. To what extent the proteins penetrate the brushes remains to be determined.

4. Experimental Section

Chemicals: *N*-isopropylacrylamide (NIPAM) and 1,1,4,7,7-pentamethyldiethylenetriamine (PMDETA) were purchased from Acros. 2-[methoxy(polyethyleneoxy)propyl]-trichlorosilane was from Gelest Inc., which includes 6–9 ethylene oxide units. CuBr, methanol, anhydrous toluene, BSA were all from Sigma-Aldrich. Bovine fibronectin was from Calbiochem. The proteins used for adsorption studies were all dissolved in phosphate buffered saline (PBS; 0.137 M NaCl, 0.01 M Na_2HPO_4, 0.0027 M KCl, and 0.002 M KH_2PO_4, pH 7.2). NIPAM monomer was re-crystallized from hexane. The initiator, 11-(2-bromo-2-methyl)-propionyl undecyl trichlorosilane, was synthesized as described.[52] All aqueous solutions were prepared with Milli-Q purified water (Millipore, Bedford, MA) with a resistivity of 18.2 MΩ cm.

Preparation of Grafted Poly(N-Isopropylacrylamide) on Silicon Substrates: The surface-initiated atom transfer radical polymerization (ATRP) was used to synthesize PNIPAM on initiator-functionalized silicon substrates, as described.[22] In brief, silicon wafers or glass slides were first cleaned in piranha solution (25% (v/v) hydrogen peroxide and 75% (v/v) sulfuric acid) at 60 °C for 1 h. *Warning: piranha solution can react strongly with organic compounds. It should be handed with extreme caution and it should not be stored in closed containers.* After rinsing with deionized water and drying under a stream of nitrogen, the clean silicon substrates were immersed in a toluene solution containing 2 mM mixtures of the initiator and OEG for 4 h, to form self-assembled monolayers of the initiator (SAM-Br) and 2-[methoxy(polyethyleneoxy)propyl]-trichlorosilane (SAM-OEG). The substrates were then cleaned with toluene, ethanol, and deionized (DI) water in an ultrasonic bath for 3 min each and dried with nitrogen. To obtain substrates with different SAM-Br surface densities, the monolayers were assembled from solutions with different molar percentages of SAM-Br and SAM-OEG. The initiator density resulting from the different mixtures was described previously.[22]

PNIPAM was synthesized from substrates functionalized with SAM-Br or with a SAM-Br:SAM-OEG mixture, in the reaction vessel. The vessel was first degassed with three freeze-pump-thaw cycles, after the substrate loading. Degassed NIPAM monomer solution (3.955 g, 35 mmol in a mixture of MeOH/H_2O [v/v: 7/3]), the catalyst of CuBr (50.75 mg, 0.35 mmol), and the PMDETA ligand (227.92 catalyst mmol), were then transferred into the reaction vessel via a cannula. The polymerization reaction was at room temperature under a nitrogen atmosphere, for the specified times needed to achieve a desired MW. After the reaction, the samples were rinsed with methanol, followed by sonication in methanol, ethanol, and water, and finally dried with filtered nitrogen.

Thickness of PNIPAM Films Determined by Ellipsometry: A Gaertner ellipsometer (Model L116C) and LGEMP software (Gaertner Scientific Corp, USA) were used to measure the thickness of the dry PNIPAM films. The 632.8 nm light was set at an incident angle of 70° in all experiments. The single-layer box model was used to fit the data, in order to determine the PNIPAM film thickness on the silicon wafer. The

refractive index and extinction coefficient of the clean silicon wafer were 3.85 and –0.02, respectively. The refractive index of 1.46 was used for the measured organic layer thickness in air. Six different positions were measured on each sample to obtain the average thickness and standard deviation.

Characterization of PNIPAM Surface Composition: XPS (Kratos Axis ULTRA spectrometer) was used to measure the surface chemical composition of modified silicon substrates. The excitation source was the monochromatic Al K_α radiation at 1486.6 eV (225 W, 40 eV pass energy). The samples were loaded on a rectangular metal support, using double-sided adhesive tape, and analyzed at a pressure of 10^{-9} Torr. To measure the binding energy, the C 1s hydrocarbon peak at 285.0 eV was used as the reference peak. Surface chemical compositions were determined from the integrated peak areas in the XPS spectra.

Assessment of Reversible Cell Attachment: Cell adhesion on PNIPAM grafted surfaces was evaluated in vitro by culturing NIH 3T3 fibroblasts on PNIPAM-coated substrates. Cells in a humidified incubator with 5% CO_2 at 37 °C were cultured in Dulbecco's modified Eagle's medium (DMEM), supplemented with 10 v/v% fetal bovine serum (FBS), 100 units mL^{-1} penicillin, and 100 µg mL^{-1} streptomycin. The cells were initially harvested from cell culture flasks with a 0.1% trypsin solution. For cell attachment assays, the square, PNIPAM-coated glass slides (15 × 15 mm) were first placed in a tissue culture dish. Then harvested cells were seeded into the dish at 1×10^4 cells cm^{-2}, and the dish was placed in the incubator. After 24 h in culture, phase contrast images of adhered cells on the PNIPAM-coated substrata were observed with a Zeiss Axiovert 200 M microscope (Thornwood, NY) equipped with a temperature controlled stage. In each case, we evaluated the density of attached cells, their spread areas, and their circularity. To assess the temperature-driven reversibility of cell attachment, after 24 h in culture, the warm medium (37 °C) was gently aspirated away, and replaced with L-15 medium at room temperature (≈23 °C). The cells were then cultured at room temperature on the PNIPAM films, and imaged 30 min, 90 min, and 180 min after replacing the medium and reducing the temperature.

Cell attachment was quantified according to the number of adhered cells per area. For each PNIPAM coating sample, six images were analyzed to obtain the average and standard deviation. Both the spread area and circularity of individual cells in the image were also determined, using the Freehand Tool in ImageJ (v1.43). In the latter two cases, for each sample, 50 cells were analyzed, to obtain the representative statistics.

The LCST of PNIPAM is altered slightly by the cell culture medium and by PBS, compared to pure water. Prior studies showed that 0.12 M NaCl and 0.01 M phosphate decreased the LCST by <2 °C and 0.2 °C, respectively.[53,54] However, even with these small changes, the measurements at 23 °C and 37 °C were well outside the transition range, and would be unaffected.

Protein Adsorption: Protein adsorption was quantified with two model proteins: BSA and fibronectin. They were labeled with the isotope of ^{125}iodine (^{125}[I]-BSA and ^{125}[I]-FN), as described previously.[22] Iodobeads (Pierce) were used to label proteins with carrier free Na^{125}[I] (Perkin Elmer). The unbound ^{125}[I] was removed with a PD-10 desalting column (GE Healthcare Bioscience) and the determined specific activity of iodinated proteins was around 20 cpm ng^{-1}.

To carry out the protein adsorption measurements, a SecureSeal Imaging Spacer (Grace Biolabs) with a 13 mm circular cutout was affixed to the PNIPAM-coated substrate. This allowed exposure of a well-defined sample area to protein solution. ^{125}[I] labeled protein (^{125}[I]-BSA, 200 µL, 1 mg mL^{-1}; or ^{125}[I]-FN, 200 µL, 0.05 mg mL^{-1}) was then layered onto the exposed sample and incubated with the sample for 2 h at either 23 °C (room temperature) or at 37 °C in an incubator. Because protein adsorption on PNIPAM reportedly saturates within 2 h,[1] the 2 h incubation time was chosen for the protein adsorption study. After the incubation, the sample was rinsed ten times by gently aspirating away the solution and displacing the protein solution with 100 mL aliquots of buffer. The buffer used was maintained at the incubation temperature. For example, for samples incubated at 37 °C, the buffer and sample were maintained at 37 °C during all rinsing steps. After rinsing and air-drying, the samples were placed in scintillation vials with 5 mL of scintillation cocktail. The counts were measured with an LS 6500 scintillation counter (Beckman Instruments) with the manufacturer-specified settings for ^{125}iodine detection. Four replicate samples were tested for each coating and control measurements were carried out with silicon samples coated with oligoethylene oxide-terminated silane.

Supporting Information

Supporting Information is available from the Wiley Online Library or from the author.

Acknowledgements

This work was supported by the National Science Foundation under NSF Award Number DMR 08-04113.

Received: December 16, 2011
Revised: January 26, 2012
Published online: March 15, 2012

[1] D. L. Huber, R. P. Manginell, M. A. Samara, B. I. Kim, B. C. Bunker, *Science* **2003**, *301*, 352.
[2] J. Wongkongkatep, R. Ladadat, W. Lappermpunsap, P. Wongkongkatep, P. Phinyocheep, A. Ojida, T. Hamachi, *Chem. Lett.* **2010**, *39*, 184.
[3] P. S. Stayton, T. Shimoboji, C. Long, A. Chilkoti, G. Chen, J. M. Harris, A. S. Hoffman, *Nature* **1995**, *378*, 472.
[4] Y. Hu, T. Kaoru, *Colloid Surf. B* **2005**, *46*, 142.
[5] I. Y. Galaev, B. Mattiasson, *Trends Biotechnol.* **1999**, *17*, 335.
[6] H. Kanazawa, Y. Kashiwase, K. Yamamoto, Y. Matsushima, A. Kikuchi, Y. Sakurai, T. Okano, *Anal. Chem.* **1997**, *69*, 823.
[7] E. Ayano, Y. Okada, C. Sakamoto, H. Kanazawa, A. Kikuchi, T. Okano, *J. Chromatogr.* **2006**, *1119*, 51.
[8] H. Yamanaka, K. Yoshizako, Y. Akiyama, H. Sota, Y. Hasegawa, Y. Shinohara, A. Kikuchi, T. Okano, *Anal. Chem.* **2003**, *75*, 1658.
[9] A. Mizutani, K. Nagase, A. Kikuchi, H. Kanazawa, Y. Akiyama, J. Kobayashi, M. Annaka, T. Okano, *J.Chromatogr. B Anal. Technol. Biomed. Life Sci.* **2010**, *878*, 2191.
[10] H. A. von Recum, S. W. Kim, A. Kikuchi, M. Okuhara, Y. Sakurai, T. Okano, *J. Biomed. Mater. Res.* **1998**, *40*, 631.
[11] N. Ozturk, A. Girotti, G. T. Kose, J. C. Rodriguez-Cabello, V. Hasirci, *Biomaterials* **2009**, *30*, 5417.
[12] T. Ohki, M. Yamato, D. Murakami, R. Takagi, J. Yang, H. Namiki, T. Okano, K. Takasaki, *Gut* **2006**, *55*, 1704.
[13] Y. Shiroyanagi, M. Yamato, Y. Yamazaki, H. Toma, T. Okano, *Tissue Eng.* **2003**, *9*, 1005.
[14] Y. Tsuda, A. Kikuchi, M. Yamato, A. Nakao, Y. Sakurai, M. Umezu, T. Okano, *Biomaterials* **2005**, *26*, 1885.
[15] N. Yaji, M. Yamato, J. Yang, T. Okano, S. Hori, *Biomaterials* **2009**, *30*, 797.
[16] K. Washio, T. Iwata, M. Mizutani, T. Ando, M. Yamato, T. Okano, I. Ishikawa, *Cell Tissue Res.* **2010**, *341*, 397.
[17] J. Yang, M. Yamato, T. Okano, *MRS Bull.* **2005**, *30*, 189.
[18] J. Yang, M. Yamato, T. Shimizu, H. Sekine, K. Ohashi, M. Kanzaki, T. Ohki, K. Nishida, T. Okano, *Biomaterials* **2007**, *28*, 5033.
[19] K. N. Plunkett, X. Zhu, J. S. Moore, D. E. Leckband, *Langmuir* **2006**, *22*, 4259.
[20] X. Zhu, C. Yan, F. M. Winnik, D. Leckband, *Langmuir* **2007**, *23*, 162.

[21] H. Yim, M. S. Kent, D. L. Huber, S. Satija, J. Majewski, G. S. Smith, *Macromolecules* **2003**, *36*, 5244.
[22] C. Xue, N. Yonet-Tanyeri, N. Brouette, M. Sferrazza, P. V. Braun, D. E. Leckband, *Langmuir* **2011**, *27*, 8810.
[23] M. Hirose, M. Yamato, O. H. Kwon, M. Harimoto, A. Kushida, T. Shimizu, A. Kikuchi, T. Okano, *Yonsei Med. J.* **2000**, *41*, 803.
[24] A. Mizutani, A. Kikuchi, M. Yamato, H. Kanazawa, T. Okano, *Biomaterials* **2008**, *29*, 2073.
[25] H. E. Canavan, X. Cheng, D. J. Graham, B. D. Ratner, D. G. Castner, *Langmuir* **2005**, *21*, 1949.
[26] Y. Akiyama, A. Kikuchi, M. Yamato, T. Okano, *Langmuir* **2004**, *20*, 5506.
[27] H. Yim, M. S. Kent, S. Mendez, S. S. Balamurugan, S. Balamurugan, G. P. Lopez, S. Satija, *Macromolecules* **2004**, *37*, 1994.
[28] H. Yim, M. S. Kent, S. Satija, S. Mendez, S. Balamurugan, S. S. Balamurugan, G. P. Lopez, *J. Polym. Sci. B* **2004**, *42*, 3302.
[29] L. Li, Y. Zhu, B. Li, C. Gao, *Langmuir* **2008**, *24*, 13632.
[30] B. Kong, J. S. Choi, S. Jeon, I. S. Choi, *Biomaterials* **2009**, *30*, 5514.
[31] R. M. da Silva, J. F. Mano, R. L. Reis, *Trends Biotechnol.* **2007**, *25*, 577.
[32] K. Fukumori, Y. Akiyama, M. Yamato, J. Kobayashi, K. Sakai, T. Okano, *Acta Biomater.* **2009**, *5*, 470.
[33] H. Takahashi, M. Nakayama, M. Yamato, T. Okano, *Biomacromolecules* **2010**, *11*, 1991.
[34] H. Yim, M. S. Kent, S. Mendez, G. P. Lopez, S. Satija, Y. Seo, *Macromolecules* **2006**, *39*, 3420.
[35] A. Halperin, M. Kroger, *Langmuir* **2009**, *25*, 11621.
[36] A. Halperin, G. Fragneto, A. Schollier, M. Sferrazza, *Langmuir* **2007**, *23*, 10603.
[37] A. Halperin, M. Kroger, E. B. Zhulina, *Macromolecules* **2011**, *44*, 3622.
[38] T. McPherson, A. Kidane, I. Szleifer, K. Park, *Langmuir* **1998**, *14*, 176.
[39] I. Szleifer, *Biophys. J.* **1997**, *72*, 595.
[40] A. Halperin, *Langmuir* **1999**, *15*, 2525.
[41] D. W. Sindorf, G. E. Maciel, *J. Phys. Chem.* **1982**, *86*, 5208.
[42] D. Sunday, S. Curras-Medina, D. L. Green, *Macromolecules* **2010**, *43*, 4871.
[43] H. Tu, C. E. Heitzman, P. V. Braun, *Langmuir* **2004**, *20*, 8313.
[44] J. Israelachvili, *Intermolecular and Surface Forces*, 2 ed., Academic Press, New York **1992**.
[45] D. C. Carter, J. X. Ho, *Adv. Protein Chem.* **1994**, *45*, 153.
[46] J. Satulovsky, M. A. Carignano, I. Szleifer, *Proc. Natl. Acad. Sci. U S A* **2000**, *97*, 9037.
[47] B. Zhu, T. Eurell, R. Gunawan, D. Leckband, *J. Biomed. Mater. Res.* **2001**, *56*, 406.
[48] X. Zhu, J. Degraaf, F. M. Winnik, D. Leckband, *Langmuir* **2004**, *20*, 10648.
[49] H. E. Canavan, D. J. Graham, X. Cheng, B. D. Ratner, D. G. Castner, *Langmuir* **2007**, *23*, 50.
[50] K. Fukumori, Y. Akiyama, Y. Kumashiro, J. Kobayashi, M. Yamato, K. Sakai, T. Okano, *Macromol. Biosci.* **2010**, *10*, 1117.
[51] S. Burkert, E. Bittrich, M. Kuntzsch, M. Muller, K. J. Eichhorn, C. Bellmann, P. Uhlmann, M. Stamm, *Langmuir* **2010**, *26*, 1786.
[52] K. Matyajaszewski, P. J. Miller, N. Shukla, B. Immaraporn, A. Gelman, B. B. Luokala, T. M. Siclovan, G. Kickelbick, T. Vallant, H. Hoffmann, T. Pakula, *Macromolecules* **1999**, *32*, 8716.
[53] Y. K. Jhon, R. R. Bhat, C. Jeong, O. J. Rojas, I. Szleifer, J. Genzer, *Macromol. Rapid Commun.* **2006**, *27*, 697.
[54] Y. Zhang, S. Furyk, L. B. Sagle, Y. Cho, D. E. Bergbreiter, P. S. Cremer, *J. Phys. Chem. C* **2007**, *111*, 8916.